Reducing Visible Staircasing Artifacts Through Printing Orientation Using a Perception-Driven Metric

M. A. Yurtsever ¹ and P. Didyk ¹

¹Università della Svizzera italiana, Switzerland

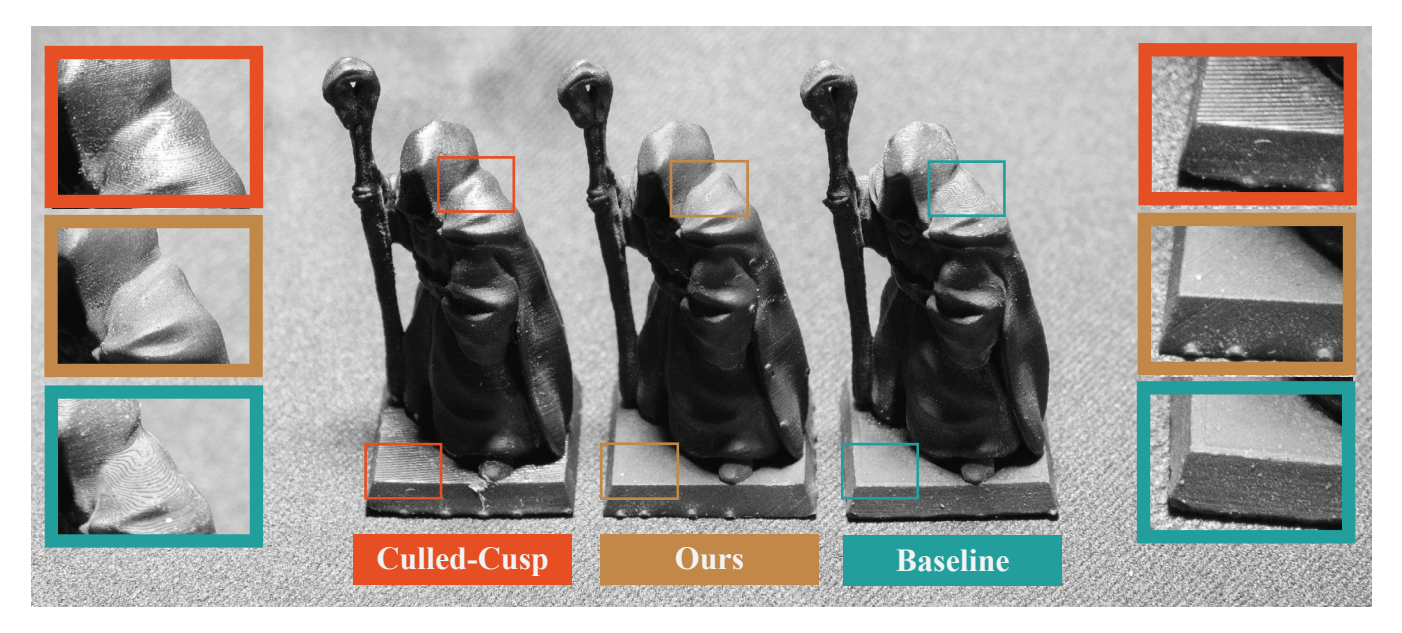


Figure 1: We study surface artifacts created in the 3D printing process. These staircasing artifacts and their relation to printing orientation are examined. We propose a method for optimizing the printing orientation to reduce visible staircasing artifacts. In the figure you can see these artifacts on the HOODED STRANGER model printed with SLA in different orientations.

Abstract

3D printing is widely used for prototyping and fabricating custom designs. Due to the discretization introduced during printing, the quality of the fabricated surfaces often suffers from so-called staircasing artifacts. While all 3D printers produce these artifacts, their severity depends on the printing resolution. Thus, these artifacts are particularly pronounced in low- to medium-cost printers, which are commonly used by home users, hobbyists, and enthusiasts of 3D printing. Changing the printing orientation allows for reducing the artifacts, enabling more accurate surface reproduction. While several previous works exploited this idea, they formulated the problem based on the geometrical accuracy of surface reproduction. This paper takes a different approach that focuses on the perception of the surface appearance. Our work is motivated by the fact that the visual severity of the artifacts depends on the characteristics of the patterns that the staircasing produces. These are also influenced by the viewing conditions, i.e., lighting and viewing orientations. Consequently, we develop in this paper a perception-inspired technique for quantifying the visibility of staircasing artifacts that takes the above factors into consideration. It is grounded in the human contrast sensitivity function, which models the ability of the human visual system to detect spatial patterns. Using the method, we propose an optimization procedure for finding the printing orientation for 3D models, which minimizes the visibility of staircasing artifacts. We evaluate our method against geometric approaches across a range of 3D models and viewing conditions. Our user study confirms the effectiveness of our approach in reducing the visual impact of staircasing artifacts.

CCS Concepts

• Computing methodologies \rightarrow Shape analysis; Mesh models; Perception;

1. Introduction

3D printers can create objects with extraordinary complexity, enabling a wide range of applications across various fields. With the recent boost in popularity among home users, 3D printers are moving away from their intended purpose of fast prototyping. With these alternative use cases, the visual appearance of the printed objects often becomes an important factor. Although printed meshes are usually expected to have smooth surfaces, the inherent limitations of 3D printers operating by depositing discrete layers of material make it difficult to achieve this smoothness. The result is the formation of artifacts known as staircasing artifacts (Figure 2), which give surfaces a jagged appearance and can diminish their visual appeal. The effect can be especially visible when 3D-printed objects are viewed from a close distance or under specific illumination.

The staircasing artifacts can be removed during a post-processing step, which can involve sanding the objects, applying vapor smoothing, or using other surface treatments. While effective, such methods are cumbersome to apply and usually destroy other features of the printed object by smoothing them. Other methods involve preprocessing printed geometry to hide the surface



Figure 2: A 3D printed model with staircasing artifacts especially visible in the cheek and in the hat.

inaccuracies [MBU22] or adaptive slicing [SHH96; AHL17], which modifies layer height according to the geometry. The methods effectively reduce the artifacts but require adapting the slicing software. Our work is similar to [WZK16], which minimizes the printed surface error by optimizing printing direction based on the geometrical error introduced in the 3D printing process. The advantage of such an approach is the simplicity of integrating such a method with any printing software.

In this work, we extend the idea of Wang et al. [WZK16] by focusing directly on the visibility of the staircasing artifacts, which depends not only on printing direction but also viewing conditions and characteristics of the staircasing patterns. The key component of our method is a perception-based metric that measures the visual severity of artifacts. Unlike the previous approach that evaluates only the volumetric difference between a mesh and its printed counterpart, our method additionally considers the viewing conditions and the contrast sensitivity function (CSF), which describes the sensitivity of the human visual system (HVS) to simple patterns. By leveraging the limitations of the HVS modeled by the metric, our method optimizes printing direction to make the staircase artifacts less visible to observers or to position them in less noticeable areas of the model. We showcase the effectiveness of optimizing printing direction using our metric on various objects printed using an SLA printer. We also compare our perception-based approach to the previous method in a series of user experiments demonstrating the advantages of using our method.

2. Related Work

Adaptive slicing is one of the most common ways to improve the accuracy of fabricated surfaces and remove staircasing artifacts by adapting layer height to reduce printing errors. Most methods range from local, that adjust the slice height based on the local error [DM94], to methods that try to apply coarse-to-fine [HRJ97] or fine-to-coarse approaches [HA13]. These methods aim to balance the printing speed and accuracy by starting from thick layers and then subdividing them if needed or vice versa, starting from very fine layers and then merging them based on the produced error usually defined by the volume error [TFBA98]. More advanced techniques solve the problem using a global optimization approach [WCT*15; AHL17]. The above methods apply to almost all layered fabrication methods where variable layer height is possible. Some of them are also integrated into printing software, such as Prusa [Pru]. However, their efficiency in addressing staircasing artifacts is limited by the minimum layer height that can be produced. This remains true also for more advanced methods, such as [ERP*19; SRSL17], where the layer height can be modulated within one layer. Such approach is additionally limited to printing methods that have such capabilities like FDM printers. Similarly, multi-axis printers are utilized for their ability to change the printing orientation on the fly[KO13]. This ability can be used to create support-free structures [DWW*18] or with the introduction of curved slicing, reduce surface artifacts[ZFH*22; LZC*24]. However, these methods are applicable to specifically to multi-axis printers that are not commonly accessible.

Another approach to alter the reproduction of printed objects is to change the printing direction. The strategy has been applied, for example, to optimize the surface roughness and printing time [TPR04], tensile strength [SMS13; SOM09], and to hide the support structure artifacts [ZLP*15; FAG*20]. Changing the printing direction has also been successfully applied to improve the accuracy of the printed surfaces. In this context, the most related to our work is the work of Wang et al. [WZK16], who proposed to divide models into subparts and optimized the printing direction for each of them to maximize surface reproduction. Similarly to many adaptive slicing techniques, this method relies on volumetric error measure based on the cusp height. Cusp error method, defines the error in relation to the distance between the printed surface and the ideal surface. In our work, we demonstrate that if visual appearance is highly important, such an error definition is suboptimal, and better results can be obtained by considering perceptual aspects. While optimal printing direction is usually addressed in isolation from adaptive slicing, the two can also be combined [XWL*97].

Recently, Morsy et al. [MBU22] addressed staircasing artifacts by taking inspiration from visual perception. Similarly to our work, they exploited the fact that the HVS is less sensitive to high spatial frequency and proposed modifying the printed surfaces' local microstructure to make the artifacts less apparent. The method was integrated into the poly-jet printing software. While our work addresses the same problem and draws inspiration from similar observations, we take a different approach. We follow the previous work on finding optimal printing direction, making our method easy to integrate with any printing system and not requiring explicit modification to the printed geometry.

3. Error for a Plane in Space

We propose a novel error metric for staircasing artifacts that consider human perception. To establish a basis for our method, we start by analyzing the staircasing errors for any arbitrary plane in space, before extending to meshes. This goal is encouraged by the fact that knowledge of the error for any plane in space, can easily be scaled by integrating over the surface. In this section, we outline how any 3D printed plane can be characterized by a 1D function, how to derive it algebraically, how to apply contrast sensitivity to it, and finally how to compute the error.

3.1. Character of the Artifact

Consider a plane printed in an arbitrary orientation, as shown in Figure 3, assumed to be viewed under a directional light and orthographic projection. A perfect staircase on that plane exhibits only two colors, one for the top and one for the side of the staircase independent from the illumination model. Thus to keep this simple two-value function, we consider our planes to be viewed under constant view direction and light direction. Later, we show that this assumption of directional light and orthographic projection does not need hold for meshes. We can define the function that gives the color for any point in the plane as $c': \mathbb{R}^2 \to \{c_s, c_t\}$ where c_s and c_t are the colors for the side and top of the stairstep respectively. Under that projection, this function then has the shape of bands.

Staircasing artifacts occur along the printing direction. Hence we specify the direction of occurrence as the projection of the printing direction onto the plane. Although these artifacts cover the entire plane, the form of these artifacts can be condensed to a 1D function on the direction of occurrence, as contrast variations only arise along it. By exclusively considering the color value along this line we can reduce the dimension and complexity of the color function. This occurrence direction is highlighted by a green line in Figure 3. See that a function defined in this manner exhibits a harmonic structure alternating between c_s and c_t . The computation of this error can be further simplified if we consider the original plane. An ideal smooth plane would display constant color. Hence resulting in a uniform function along the occurrence direction. Consequently we consider the function $c : \mathbb{R} \to \{0, c_t - c_s\}$, that exclusively assesses the difference between these values. We refer to this 1D function as the character of the artifact. We use the character of the artifact as our main way of analyzing planes. This observation serves as the main inspiration behind our error metric.

A straightforward solution to computing character function involves just rendering these planes, where you calculate the color for different points on the surface and compare them to the original plane. Our approach eliminates this requirement, avoiding the aliasing artifacts that can be induced by the limited resolution.

The function c as defined above is a repeating pattern of rectangular functions. We can define the function $c : \mathbb{R} \to \{0, c_t - c_s\}$ as follows.

$$c(x) = (c_t - c_s) \sum_{n = -\infty}^{\infty} \delta(x - nT) * \operatorname{rect}(\frac{2x}{S_t})$$
 (1)

Where δ is the Dirac delta function, * is the convolution operator and rect is the rectangular signal function. The function c defines a

repeating rectangular function with period T and size S_t as defined in the Figure 3. This function is also dependent on \mathbf{v} the view direction, \mathbf{l} the light direction, H the layer height and finally the N normal for the printed plane.

3.2. Error of the Character

The periodic nature of these artifacts encourages us to analyze the behavior in terms of their frequency domain representation. This also benefits our approach when we consider human perception later on. By applying the convolution theorem we find C(v), the Fourier transform of c(x), as

$$C(v) = (c_t - c_s) \sum_{n = -\infty}^{\infty} \frac{2\pi}{T} \cdot \delta\left(v - \frac{n}{T}\right) \cdot S_t \cdot \text{sinc}(S_t v), \quad (2)$$

where $\operatorname{sinc}(x) = \frac{\sin(x)}{x}$. We define the power *P* for our color function as

$$P(N) = P(\mathcal{C}) = \int_{v \in \mathbb{R}} \|(\mathcal{C}(v))\|^2 dv.$$
 (3)

See that by the definition of the Dirac delta function, C(v) = 0 for all $v \neq \frac{n}{T} \, \forall n \in \mathbb{N}$. We observe that the frequency domain representation of this power function is made of discrete points making it easier to integrate. Hence we format P as

$$P(N) = \sum_{n = -\infty}^{\infty} \left\| \mathcal{C}\left(\frac{n}{T}\right) \right\|^2 \tag{4}$$

This power is also dependent on \mathbf{v} the view direction, \mathbf{l} the light direction and the layer height H like C.

As aforementioned, under directional light and a fixed view direction, an ideal plane exhibits a constant color. Consequently, any deviations from this ideal can be considered artifacts. A function with a constant value everywhere is defined solely by a DC component (0-frequency) in the frequency domain representation. Therefore also using the symmetricity of $\mathcal C$ we can define error function E deviation from the ideal plane as

$$E(N) = P(N) - \|\mathcal{C}(0)\|^2 = 2\sum_{n=1}^{\infty} \|\mathcal{C}\left(\frac{n}{T}\right)\|^2$$

$$E(N) = 2\sum_{n=1}^{\infty} \left\|\frac{2\pi}{T}(c_t - c_s) \cdot S_t \cdot \operatorname{sinc}\left(\frac{S_t n}{T}\right)\right\|^2$$
(5)

One significant development in our understanding of human perception in modern times is the contrast sensitivity function (CSF). It defines the human visual system sensitivity to luminance modulation at different spatial frequencies [Rob66; Bar99]. To reflect the fact that human visual system sensitivity is different for different frequencies, we weight different frequency component of our error with respective sensitivity. Notably, after 60 cycles per degree CSF function can be considered 0, to create an upper limit for our error sum using Barten's CSF model[Bar03]. This allows us to avoid summing to infinity. Let us assume for a given distance 60 cycles per degree corresponds to f_m cycles per mm. Therefore our metric that considers the CSF becomes.

$$E(N) = 2 \sum_{n=1}^{\lceil f_m T \rceil} \left\| CSF\left(\frac{n}{T}\right) \cdot \frac{2\pi}{T} (c_t - c_s) \cdot S_t \cdot \operatorname{sinc} \cdot \left(\frac{S_t n}{T}\right) \right\|^2$$
 (6)

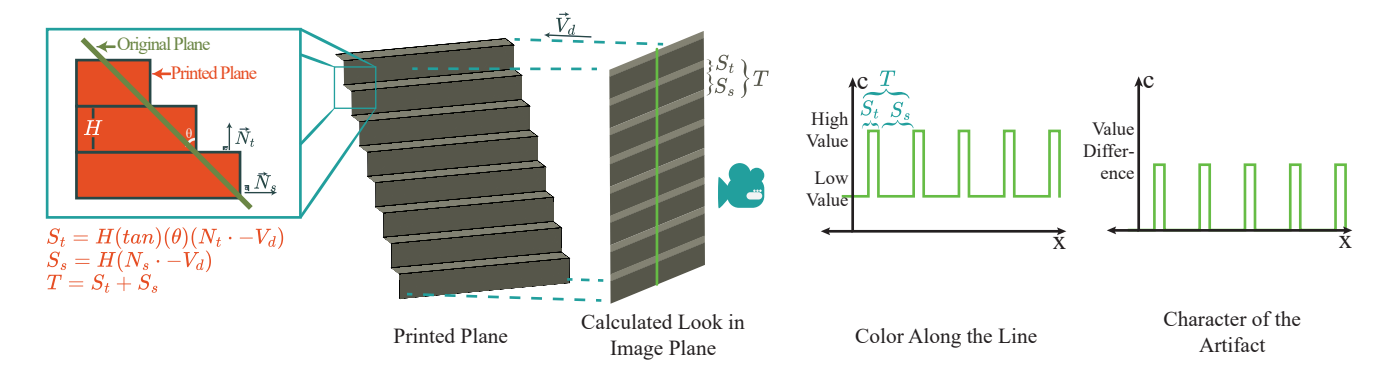


Figure 3: Under the constant light direction and view direction, a plane with a staircase has only two colors as shown. In a normal process of rendering and calculating error, the above steps must be taken. Our method skips through these to get the character of the artifact directly.

4. Error for a Model

The definition of error for an arbitrary plane in an arbitrary orientation can be easily scaled up to different types of models. When one assumes that a point, along with its normal has the error as described in the previous section, it becomes relatively simple to integrate the error across the whole model. For any given model, points on its surface are sampled and optimized over the sum of the individual errors. Although we initially considered a constant view and light direction for a plane in space, we can define the light and view directions differently for each of the sample points. Hence we use a new notation:

$$E_{L,V}(P) = E(N), \tag{7}$$

where L is the light position, V is the camera position. The error is dependent on \mathbf{l}, \mathbf{v} ; the vectors from L, V to the point P respectively. Finally N is the normal for the point P. While considering these points it is straightforward to remove these points where $\mathbf{l}, \mathbf{v} \leq 0$. See that under some viewing angles, not all sides of the staircase are visible. Under our two color assumptions, these viewing directions would show no artifacts as shown in Figure 4, hence it is rudimentary to also cull these points.

In our case, we used the STL file format commonly used in 3D printing. Where our points are defined by the center of the triangle, normals being the normal for the triangle and weighted by the projected area $P_V(F)$ of the triangle. Therefore we define the error for model \mathbf{M} with faces $F \in \mathbf{M}$.

$$E(\mathbf{M}) = \sum_{F \in \mathbf{M}} P_V(F) E_{L,V}(F)$$
(8)

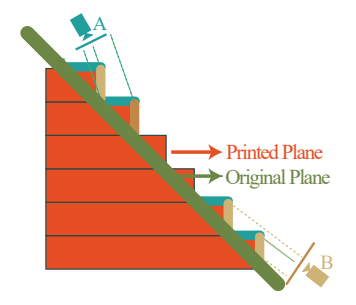


Figure 4: When viewed from some angles, not all sides of a staircase is visible; giving a sense of lack of artifacts.

4.1. Optimization

Our objective is to determine the rotation angles $\theta(pitch)$, γ (roll) in Euler angles. We consider that the printing direction is always positive z. Euler angles were chosen over quaternions because they are more commonly used in printing applications. We define a generic optimization using

$$\mathbf{r} = (\theta, \gamma) \in \mathbb{R}^2$$

$$\underset{\mathbf{r}}{\text{minimize}} \sum_{F \in \mathbf{M}} P_V(F) E_{L^{\mathbf{r}}, V^{\mathbf{r}}}(F^{\mathbf{r}})$$
 (9)

Where $L^{\mathbf{r}}, V^{\mathbf{r}}, F^{\mathbf{r}}$ are L, V, F rotated. With this simple formulation, we can extend it to various use cases by defining \mathbf{L} and \mathbf{V} , sets of L and V. Also, we can consider a rotating model considering a set of rotations \mathbf{R} .

$$\underset{\mathbf{r}}{\text{minimize}} \sum_{L \in \mathbf{L}} \sum_{V \in \mathbf{V}} \sum_{\mathbf{r}' \in \mathbf{R}} \sum_{F \in M} P_V(F^{\mathbf{r}'}) E_{L^{\mathbf{r}},V^{\mathbf{r}}}(F^{\mathbf{r}+\mathbf{r}'}) \tag{10}$$

More details on how sets L, V, R are constructed is in the following section. For optimization we used the Nelder-Mead method for it's robustness considering that our function is 2-dimensional [NM65].

5. Results

To demonstrate the effectiveness of our method in reducing staircasing artifacts, we tested it on several models for which we optimized the printing direction for different viewing conditions. We compared our results with a baseline and optimization based on a volumetric error.

Viewing conditions Figure 5 shows four different viewing conditions considered in our tests. These conditions range from simple single-point of view and light source to more complex setups where the model is examined from multiple angles. The main scene consists of a viewer seated at a table on which objects are positioned. There are also two light sources, one located above the table (Light Source 1) and one on the side (Light Source 2), both at a 70 cm

distance from the object. We also used a rotating table and a chinrest located 20 cm from the position of the object to enable different scenarios for our experiments. In Case 1, we considered a single viewpoint (the chinrest) with the Light Source 1. In Case 2, we used Light Source 2, and allowed the viewer to move within a space around a predefined range. We modeled the range of viewing positions using a 2D Gaussian distribution with $\sigma_x = 100$ mm, for horizontal direction, and $\sigma_z = 20$ mm, for vertical direction. In cases 3 and 4, we considered the model rotating on the table and illuminated with Light Sources 1 and 2, respectively.

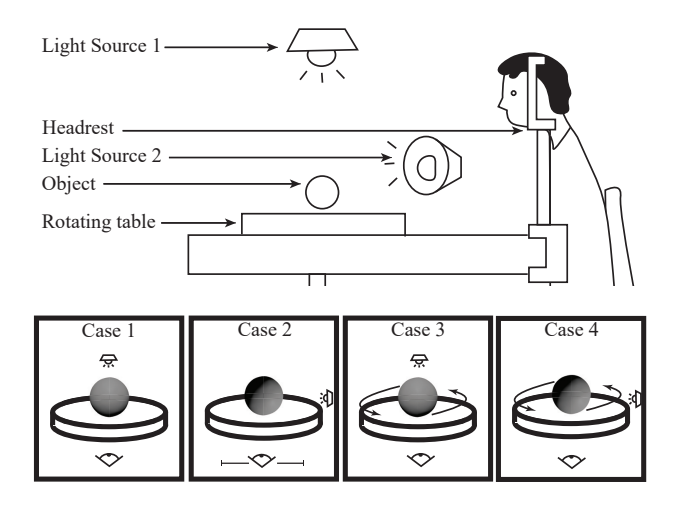


Figure 5: The figure demonstrates the experimental setup with four viewing conditions (cases) for which we optimized printing directions of our models.

Models We selected four different models shown in Figure 6 for our experiments. They were chosen to span different sizes and geometrical complexity. Using our method, we optimized the printing direction for every model and viewing condition pair (16 test cases). In cases where objects were rotating or the viewer could move, we applied a Monte Carlo sampling to compute our error function with 500 sample points for the viewing location and 60 uniformly distributed samples to sample the full rotation of an object. We also assumed a printing layer height of 100 microns, which is the setting we used for printing all the models with the Formlabs printer and Black Resin material. For material constants we picked the black-plastic-soft material from the MERL database [MPBM03; NDM05]. Color value computation is done using the simple Phong model.

We fabricated each model in orientations optimized for the specified viewing conditions, resulting in a total of 16 prints. Additionally, we employed three different methods for comparison. The first method, *baseline*, is printed as the standing orientation. This orientation was chosen as the most natural for printing models. The second method, *cusp*, optimizes the printing orientation for volumetric accuracy. This is similar to work by Wang et al. [WZK16] with the exception that we did not consider breaking our objects into multiple parts. For these two versions, because it is independent of the viewing condition, one object was printed for each test

model resulting in 8 prints. The third method, *culled-cusp*, again minimizes the volumetric error but discards invisible faces as our method does. For this version an object was printed for each modelview condition pair, resulting in another 16 prints.



Figure 6: *Models selected for our experiments.*

Discussion While all the fabricated models were tested in a user study (Section 6), we demonstrated only a subset of them here. We also refer to the supplementary video for better visualization of the printed results. It also important to note that viewing the results in the paper or in the video does not correspond to observing the models under the viewing conditions that were assumed for the optimization. Consequently, the ultimate validation is with human subjects. Figure 7 demonstrates the FRENCHIE model printed in directions optimized for Case 2 and Case 4. Apart from our results, the figure contains the corresponding views for the baseline and culled-cusp solutions. Note that in the baseline case, the printing direction does not depend on the viewing conditions. Therefore, we present one set of images for each of these methods. Also, in Case 2 for ours and the *culled-cusp*, the side view is not a part of the viewing condition. Our method successfully limits the staircasing artifacts or move them to the invisible regions (side view in Case 2). Interestingly, it can redistribute the artifacts when optimized for rotating object (Case 4). It is something that is not achieved when the printing direction is optimized only for the front view (Case 2). Figure 8 shows in a similar way the results for model BEAR and Case 1 and 3. Additionally, it contains plots of our error function and location in its landscape corresponding to different solutions. One can observe how the error function changes shape between different viewing conditions and suboptimal printing direction of baseline, cusp and culled-cusp methods.

Finally, Figure 9 demonstrates on HOODEDSTRANGER model how our method shifts the staircasing artifacts to surfaces that are either not visible or viewed at the grazing angle. In this case, the printing direction was optimized for the front view, which does not exhibit any artifacts. The artifacts become apparent when looking at the object from the wrong direction (e.g., side view). This behavior is similar to Case 2 in Figure 9.

Timings library. Table 1 contains running times for optimizing printing direction for Case 1 using an Intel i9700k CPU.

6. User Study

To verify whether our method indeed improved the perceived quality of printed objects, we conducted a user experiment during which

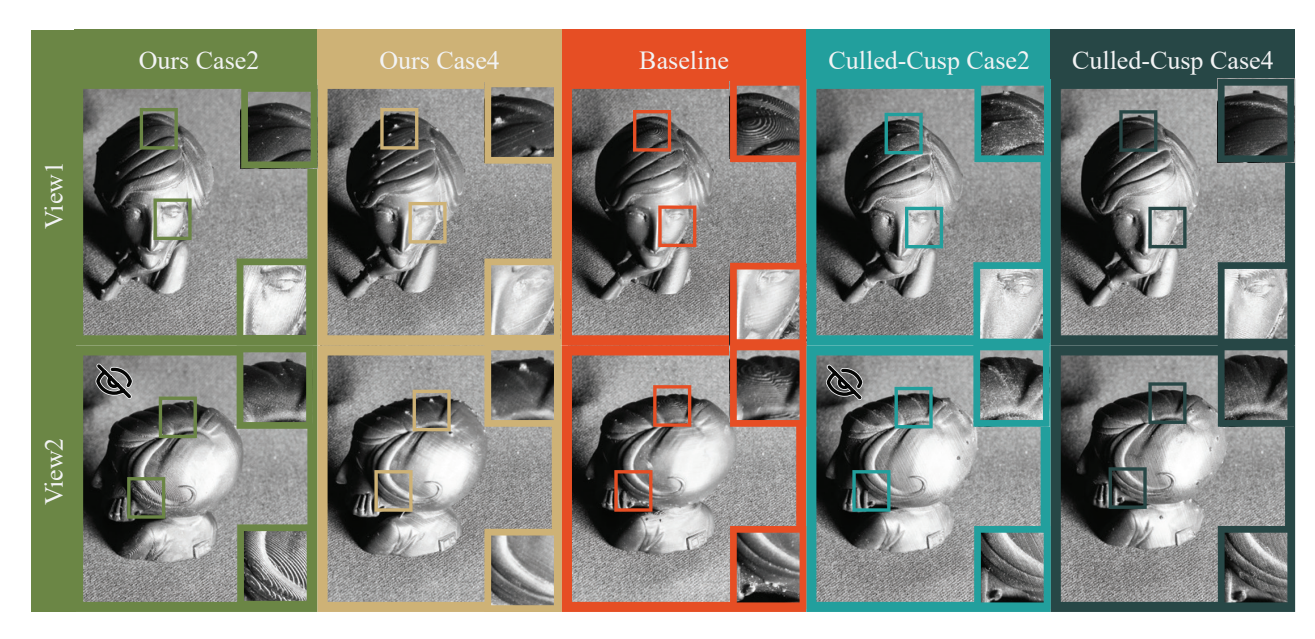


Figure 7: FRENCHIE model printed with direction optimized for Cases 2 and 4 compared to the baseline and culled-cusp solutions. Note that the artifacts in the form of little bumps on the objects' surfaces come from supporting structures and were not the subject of our optimization.

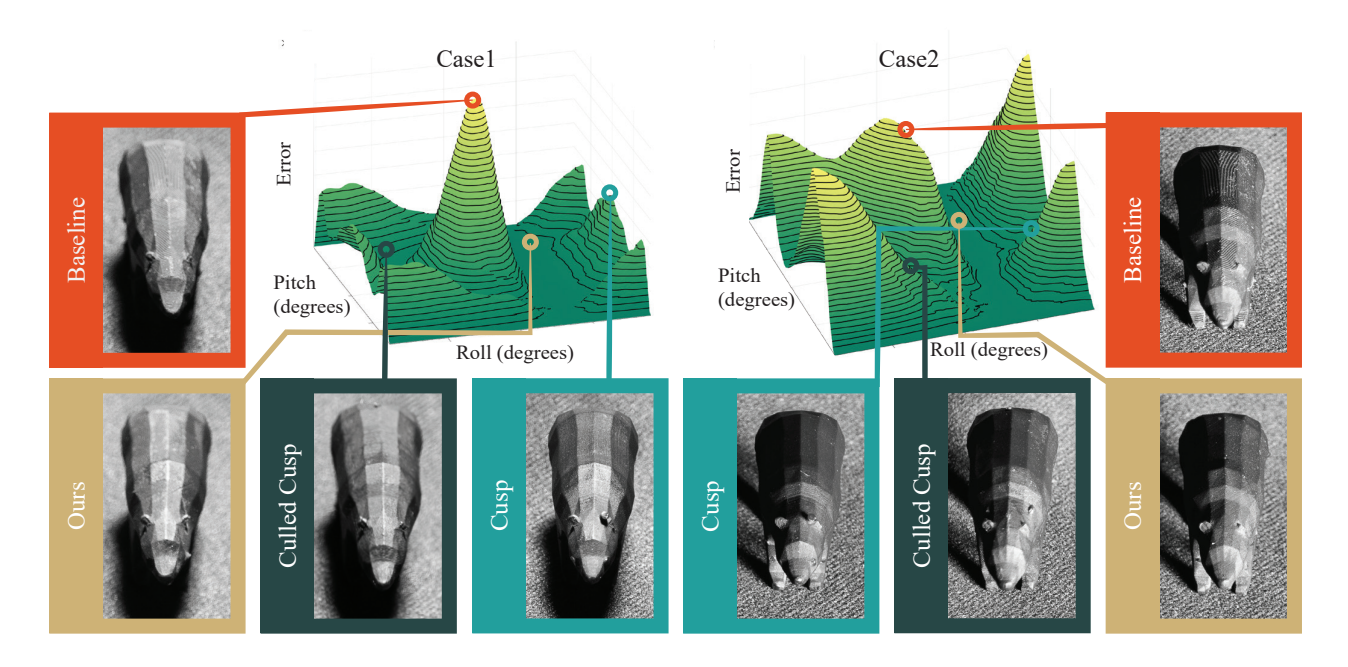


Figure 8: BEAR model printed for different cases compared to the baseline, cusp and culled-cusp solutions. See that under different lighting conditions visibility of artifacts changes. This change can be examined in the face of the model printed according to cusp.

our optimized prints were compared to their baseline, cusp and culled-cusp counterparts.

Stimuli In our experiment, we considered all viewing conditions (Figure 5) and all models (Figure 6). Each object printed according to our method was compared to corresponding *baseline*, *cusp*

and *culled-cusp* solutions. Each comparison was conducted under the conditions our method and *culled-cusp* considered for finding the optimal printing direction. As a result, each participant completed a total of 48 comparisons (4 models, 4 viewing conditions, comparison agains 3 methods).



Figure 9: HOODED STRANGER model printed for Case 2 is shown in the figure. Our method excels at pushing artifacts to hidden areas. In this case left side of the model is in shadow, hence our method pushes artifacts onto this area. See that these errors are not visible from the optimized view point.

| Model | Face Count | Iterations | Opt. Time |
|-----------------|------------|------------|-----------|
| HOODED STRANGER | 425302 | 46 | 337.3 s |
| FRENCHIE | 115391 | 47 | 102.7 s |
| JUSTCHILLING | 153836 | 54 | 142 s |
| BEAR | 946 | 63 | 3 s |

Table 1: *Optimization times for different models.*

Task At the beginning of the experiment, each participant received a brief introduction about staircasing artifacts. Other artifacts such as support artifacts were also introduced. Participants were shown samples of different models with these artifacts and were asked to judge staircasing artifacts only. In each trial, two printed models were placed in the scene according to the particular viewing condition, and the participants were asked to select the model that exhibited the least amount of staircasing artifacts. The order of presented models, methods, and viewing conditions was randomized, and each participant had unlimited time to observe the models before answering. All participants were able to finish the experiment within 40 minutes.

Participants 10 participants (7M and 3F, aged 24-32) with normal or corrected-to-normal vision took part in the experiment. They were recruited on a university campus and received financial compensation for their time.



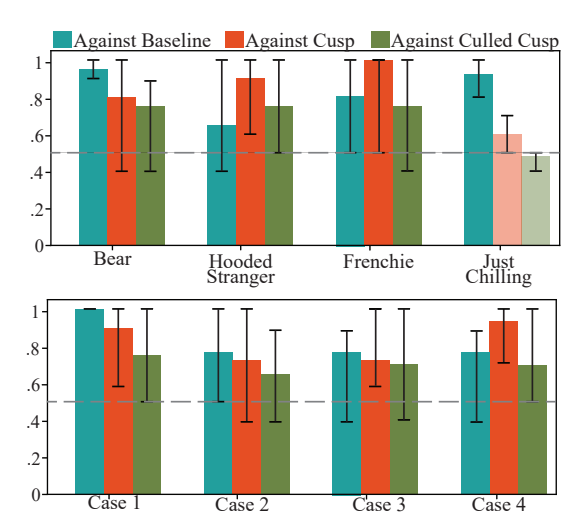


Figure 10: Preference of our method compared to baseline, cusp and culled-cusp. Whisker ends show the minimum and maximum preference for a given model out of the view cases and preference for a given view case out of different models.

Result We collected 480 comparisons and aggregated them across different viewing conditions and models. Figure 10 presents the plots of the percentage of cases in which our solution was preferred over the two other methods. In all cases, most of the participants preferred our solution. The rate of preference varies with viewing conditions and geometry, which is expected as the degree to which the staircasing artifacts can be mitigated depends on these factors. Overall, our method was chosen in 70.6% of cases when compared to the culled-cusp method, in 82.5% of cases when compared to the cusp method, in 83.1% when compared to baseline. For all cases shown in Figure 10, we performed the binomial test, which indicated that all our results are statistically significant (p-value < .00001) apart from two cases in which our method was compared to cusp and culled-cusp methods for JUSTCHILLING model (faded bars in the figure). Despite the lack of statistical difference in this case, our approach was preferred 60% of the time against cusp and 47.5% of the time against culled-cusp. This study demonstrates that our method, which accounts for the properties of the human visual system and viewing conditions, can significantly improve visual print quality. Interestingly, it is not only effective under highly constrained viewing scenarios, such as Case 1, where the viewer, object, and light source remain fixed, but it also performs better in more relaxed setups, where the viewer is allowed to move or when objects are viewed from all directions simulating freeviewing conditions.

7. Limitations & Future Work

Even though our model provides a way of estimating errors on surfaces, our staircase model is not a perfect representation of some printing methods. For instance, FDM printing results in curved edges for layers. In such cases, we need a different representation for the color along the occurrence direction. This representation

differs from the simple 2-value function we propose. Extending our approach to accommodate other printing methods is an important venue for future research.

Additionally, our method considers the ideal representation of models, but inherently fine details are often lost in 3D printing. Features smaller than the printer's resolution are approximated by the slicing algorithm. This can be addressed by integrating our method with the slicing algorithm. Additionally, this way our method can be easily extended into considering adaptive slicing or curved slicing by evaluating different layer heights for each face during optimization.

Our method only considers CSF for modeling human perception. While CSF in itself can define a range of human sensitivity, our approach can benefit from consideration of other perceptual factors. Extending our approach to consider factors such as visual masking can improve our method in the future.

We demonstrated performance of our method using single printing material. However, we believe our method is applicable to other opaque materials. Materials with significant subsurface scattering properties would require different modeling of the character function, which would not be piece-wise constant in these cases.

Any method that requires an error metric for staircasing artifacts can use our proposed error. Especially any work that already considers cusp height for error, can be made to consider perceived error by replacing the cusp height with our proposed error. Additionally integrating our approach with works that hide supporting structure artifacts or weighting our errors according to saliency would be an interesting direction for future research.

8. Conclusion

This paper proposes a novel method for reducing the visibility of staircasing artifacts on 3D-printed surfaces. The key component of the technique is a perceptually based visibility measure of these artifacts derived from the contrast sensitivity function. We first demonstrate how this perceptual error can be defined for a simple plane and then show how it can be applied to optimize the printing direction that minimizes staircasing artifacts. Our method enables optimization of the printing orientation for models without requiring any pre- or post-processing. Our experiments demonstrate a preference for our results over baseline methods and previous techniques that rely on geometric error for similar optimization. Consequently, this showcases that when visual appearance is important, considering the properties of the human visual system can enhance the 3D printing process.

References

- [AHL17] ALEXA, MARC, HILDEBRAND, KRISTIAN, and LEFEBVRE, SYLVAIN. "Optimal Discrete Slicing". ACM Trans. Graph. 36.1 (Jan. 2017). ISSN: 0730-0301. DOI: 10.1145/2999536. URL: https://doi.org/10.1145/29995362.
- [Bar03] BARTEN, PETER GJ. "Formula for the contrast sensitivity of the human eye". *Image Quality and System Performance*. Vol. 5294. SPIE. 2003, 231–238 3.
- [Bar99] BARTEN, PETER GJ. Contrast sensitivity of the human eye and its effects on image quality. SPIE press, 1999 3.

- [DM94] DOLENC, A. and MÄKELÄ, I. "Slicing procedures for layered manufacturing techniques". *Computer-Aided Design* 26.2 (1994), 119–126. ISSN: 0010-4485. DOI: https://doi.org/10.1016/0010-4485(94)90032-9. URL: https://www.sciencedirect.com/science/article/pii/00104485949003292.
- [DWW*18] DAI, CHENGKAI, WANG, CHARLIE C. L., WU, CHENMING, et al. "Support-free volume printing by multi-axis motion". *ACM Trans. Graph.* 37.4 (July 2018). ISSN: 0730-0301. DOI: 10.1145/3197517. 3201342. URL: https://doi.org/10.1145/3197517. 3201342.2.
- [ERP*19] ETIENNE, JIMMY, RAY, NICOLAS, PANOZZO, DANIELE, et al. "CurviSlicer: slightly curved slicing for 3-axis printers". ACM Trans. Graph. 38.4 (July 2019). ISSN: 0730-0301. DOI: 10.1145/3306346. 3323022. URL: https://doi.org/10.1145/3306346. 3323022 2.
- [FAG*20] FILOSCIA, IRENE, ALDERIGHI, THOMAS, GIORGI, DANIELA, et al. "Optimizing Object Decomposition to Reduce Visual Artifacts in 3D Printing". Computer Graphics Forum 39.2 (May 2020). URL: http://vcg.isti.cnr.it/Publications/2020/FAGMCC20 2.
- [HA13] HAYASI, MOHAMMAD T and ASIABANPOUR, BAHRAM. "A new adaptive slicing approach for the fully dense freeform fabrication (FDFF) process". *Journal of Intelligent Manufacturing* 24 (2013), 683–694 2.
- [HRJ97] HOPE, R.L., ROTH, R.N., and JACOBS, P.A. "Adaptive slicing with sloping layer surfaces". *Rapid Prototyping Journal* 3.3 (1997). Cited by: 115, 89–98. DOI: 10 . 1108 / 13552549710185662. URL: https://www.scopus.com/inward/record.uri?eid=2-s2.0-031333757&doi=10.1108%2f13552549710185662&partnerID=40&md5=47d45daa665d11c5070c63892e7a6a012.
- [KO13] KEATING, STEVEN and OXMAN, NERI. "Compound fabrication: A multi-functional robotic platform for digital design and fabrication". Robotics and Computer-Integrated Manufacturing 29.6 (2013), 439–448 2.
- [LZC*24] LIU, TAO, ZHANG, TIANYU, CHEN, YONGXUE, et al. "Neural Slicer for Multi-Axis 3D Printing". ACM Trans. Graph. 43.4 (July 2024). ISSN: 0730-0301. DOI: 10.1145/3658212. URL: https://doi. org/10.1145/3658212.2.
- [MBU22] MORSY, MOSTAFA MORSY ABDELKADER, BRUNTON, ALAN, and URBAN, PHILIPP. "Shape dithering for 3D printing". *ACM Trans. Graph.* 41.4 (July 2022). ISSN: 0730-0301. DOI: 10.1145/3528223.3530129. URL: https://doi.org/10.1145/3528223.35301292.
- [MPBM03] MATUSIK, W., PFISTER, H., BRAND, M., and MCMILLAN, L. "A Data-Driven Reflectance Model". ACM Transactions on Graphics (TOG) 22.3 (July 2003), 759-769. ISSN: 0730-0301. DOI: 10. 1145/882262.882343. URL: https://www.merl.com/ publications/TR2003-835.
- [NDM05] NGAN, ADDY, DURAND, FRÉDO, and MATUSIK, WOJCIECH. "Experimental Analysis of BRDF Models." *Rendering Techniques* 2005.16th (2005), 2 5.
- [NM65] NELDER, JOHN A and MEAD, ROGER. "A simplex method for function minimization". *The computer journal* 7.4 (1965), 308–313 4.
- [Pru] PRUSA. Prusa3D Slicer. http://www.prusa3d.com. [Online, Accessed: 2024-04-08] 2.
- [Rob66] ROBSON, JOHN G. "Spatial and temporal contrast-sensitivity functions of the visual system". *Journal of the optical society of America* 56.8 (1966), 1141–1142 3.
- [SHH96] SABOURIN, EMMANUEL, HOUSER, SCOTT A, and HELGE BØHN, JAN. "Adaptive slicing using stepwise uniform refinement". *Rapid prototyping journal* 2.4 (1996), 20–26 2.
- [SMS13] SAHU, RANJEET KUMAR, MAHAPATRA, SS, and SOOD, ANOOP KUMAR. "A study on dimensional accuracy of fused deposition modeling (FDM) processed parts using fuzzy logic". *Journal for Manufacturing Science & Production* 13.3 (2013), 183–197 2.

- [SOM09] SOOD, ANOOP KUMAR, OHDAR, RK, and MAHAPATRA, SIBA SANKAR. "Improving dimensional accuracy of fused deposition modelling processed part using grey Taguchi method". *Materials & design* 30.10 (2009), 4243–4252 2.
- [SRSL17] SONG, HAI-CHUAN, RAY, NICOLAS, SOKOLOV, DMITRY, and LEFEBVRE, SYLVAIN. "Anti-aliasing for fused filament deposition". *Computer-Aided Design* 89 (2017), 25–34 2.
- [TFBA98] TATA, KAMESH, FADEL, GEORGES, BAGCHI, AMIT, and AZIZ, NADIM. "Efficient slicing for layered manufacturing". Rapid Prototyping Journal 4.4 (1998), 151–167 2.
- [TPR04] THRIMURTHULU, KPPM, PANDEY, PULAK M, and REDDY, N VENKATA. "Optimum part deposition orientation in fused deposition modeling". *International Journal of Machine Tools and Manufacture* 44.6 (2004), 585–594 2.
- [WCT*15] WANG, WEIMING, CHAO, HAIYUAN, TONG, JING, et al. "Saliency-preserving slicing optimization for effective 3D printing". Computer Graphics Forum. Vol. 34. 6. 2015, 148–160 2.
- [WZK16] WANG, WEIMING M, ZANNI, CÉDRIC, and KOBBELT, LEIF. "Improved surface quality in 3D printing by optimizing the printing direction". *Computer graphics forum.* Vol. 35. 2. Wiley Online Library. 2016, 59–70 2, 5.
- [XWL*97] XU, F, WONG, YS, LOH, HT, et al. "Optimal orientation with variable slicing in stereolithography". *Rapid Prototyping Journal* 3.3 (1997), 76–88 2.
- [ZFH*22] ZHANG, TIANYU, FANG, GUOXIN, HUANG, YUMING, et al. "S3-slicer: A general slicing framework for multi-axis 3D printing". ACM Transactions on Graphics (TOG) 41.6 (2022), 1–15 2.
- [ZLP*15] ZHANG, XIAOTING, LE, XINYI, PANOTOPOULOU, ATHINA, et al. "Perceptual models of preference in 3D printing direction". *ACM Trans. Graph.* 34.6 (Nov. 2015). ISSN: 0730-0301. DOI: 10.1145/2816795.2818121. URL: https://doi.org/10.1145/2816795.28181212.